Single CeO_2 Nanowire Gas Sensor Supported with Pt Nanocrystals: Gas Sensitivity, Surface Bond States, and Chemical Mechanism

L. Liao,[†,§] H. X. Mai,[‡] Q. Yuan,[‡] H. B. Lu,[†] J. C. Li,[*,†] C. Liu,[†] C. H. Yan,[‡] Z. X. Shen,[§] and T. Yu[§]

Key Laboratory of Acoustic and Photonic Materials and Devices of Ministry of Educations, Department of Physics, Wuhan University, Wuhan 430072, China, State Key Laboratory of Rare Earth Materials Chemistry and Applications, Peking University, Beijing 100871, China, and Division of Physics and Applied Physics, School of Physical and Mathematical Sciences, Nanyang Technological University, Singapore 637616

Received: December 15, 2007; Revised Manuscript Received: March 6, 2008

We present a new type of CeO_2 nanodevice in which a single CeO_2 nanowire was used as the sensing unit. It was found that incorporation of Pt nanocrystals on CeO_2 nanowire could significantly increase the sensor response. A possible mechanism was discussed based on the study of morphology and surface bond states of the nanowire using local electron energy loss spectroscopy and X-ray photoemission spectroscopy. The results provide a pathway to improve the performance of gas sensors with a good understanding of the nanowire's surface physics and chemistry.

Introduction

Rare earth oxides have been extensively explored for several advanced applications, such as in electronics, optics, and heterogeneous catalysis, thanks to their peculiar properties arising from the availability of the 4f shell.

As a well-known functional rare earth material, ceria has been widely applied in fields such as catalysts, gas sensors, and optics due to its unique properties.[1–11] For instance, CeO_2 is adopted in three-way catalysts for reducing the emission of the toxic pollutants (CO, NO_x, and hydrocarbons, etc.) from automobile exhaust, owing to its high oxygen storage capacity, associated with its rich oxygen vacancies and low redox potential between Ce^{3+} and Ce^{4+}.[1–4] CeO_2 doped with other rare earth ions exhibits high oxide ion conductivity at a relatively low temperature (about 600 °C) and thus has been applied in solid oxide fuel cells.[5,6] Moreover, CeO_2 also has strong absorption in the ultraviolet (UV) region and is hence used as a UV blocking and shielding material.[7–9] In the above-mentioned applications, CeO_2 nanostructures show much better performance in wide areas compared to their microsized or bulk materials, owing to their considerably small sizes and large surface specific areas, as well as improved materials properties.

In this paper, we report a gas sensor using a single CeO_2 nanowire (NW) as a sensing unit. To enhance the gas sensitivity, Pt nanocrystals (NCs) were incorporated on the surfaces of CeO_2 NWs by a chemical method since the noble metal elements (Pt, Pd, Au, etc.) on the surface of a metal oxide can enhance the interaction of a reducing gas and absorbed oxygen on the surfaces.[12–14] To understand the essence of the improvement of the gas sensitivity, the bond states of CeO_2 NWs and Pt NCs were detected by electron energy loss spectroscopy (EELS) and X-ray photoemission spectroscopy (XPS). Furthermore, the gas-sensing tests show that the sensors because the Pt NCs/CeO_2 NWs have excellent potential application in the selected detection of CO. This work is one of the series of studies of our ongoing efforts toward the gas-sensing properties and applications of one-dimensional (1D) nanostructures.[15,16]

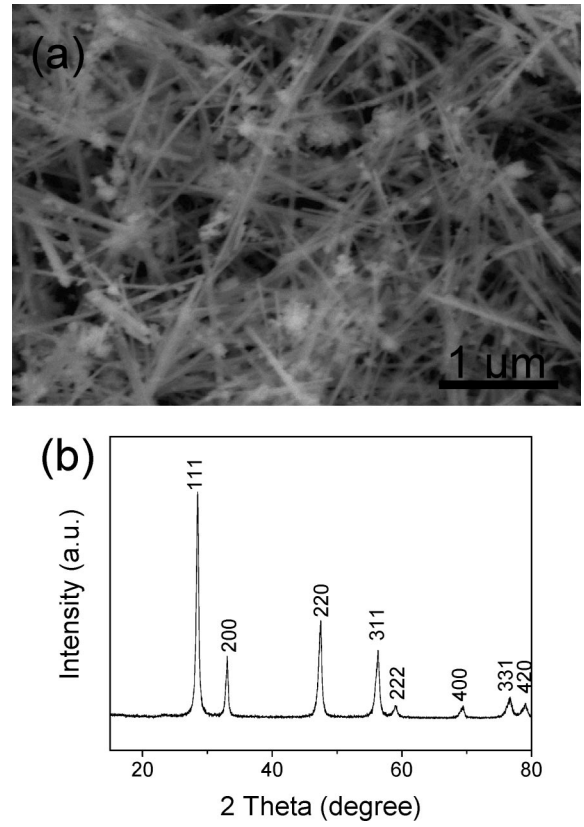

Figure 1. (a) SEM image of the CeO_2 NWs; (b) XRD pattern of the CeO_2 NWs.

Experimental Section

The CeO_2 NWs were prepared by a hydrothermal method.[17] The Pt NCs supported on the CeO_2 NWs were produced by the

* Corresponding author. E-mail: jcli@acc-lab.whu.edu.cn.
† Wuhan University.
‡ Peking University.
§ Nanyang Technological University.

10.1021/jp7117778 CCC: $40.75
Published on Web 05/21/2008

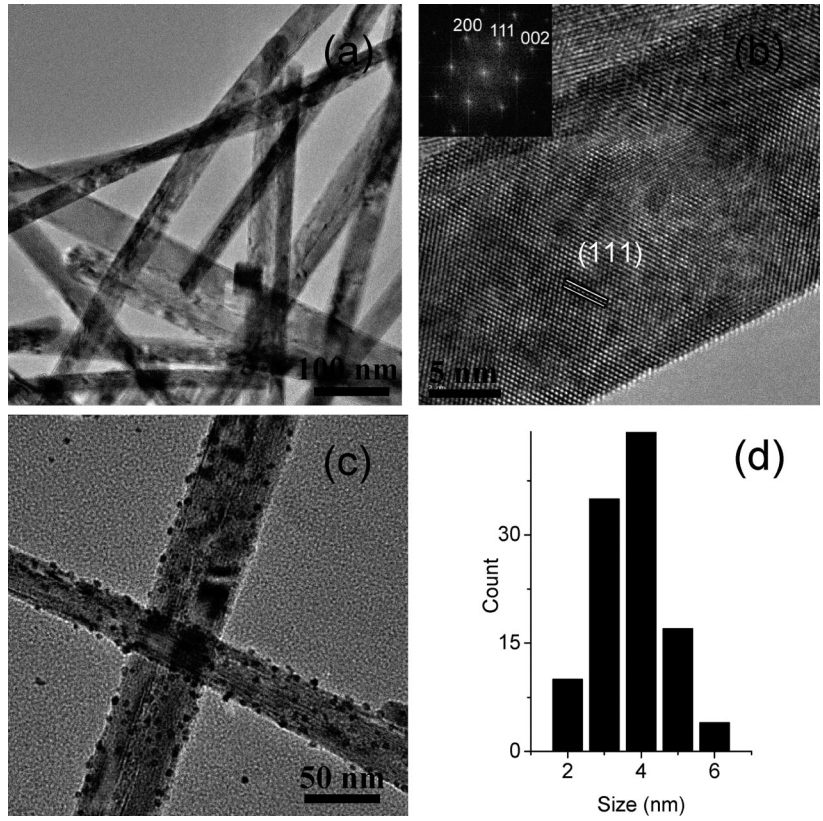

Figure 2. (a) TEM image of a bundle of CeO_2 NWs, (b) HRTEM image of a single CeO_2 NW, inset showing the FFT pattern, (c) TEM image of Pt NCs/CeO_2 NW on the carbon film of the grid, and (d) the size distribution of Pt NCs on CeO_2 NWs.

method reported in refs 18 and 19 as follows. An amount of 100 mg of poly(*N*-vinyl-2-pyrrolidone) (PVP, MW = 30 000) was dissolved in a mixture of 5 mL of 6.0 mM $H_2PtCl_6 \cdot 6H_2O$ aqueous solution, 40 mL of methanol, and 5 mL of water. The mixture was refluxed for 3 h, and then the residue was redispersed in water after the solvent was evaporated. The CeO_2 NWs (0.2 g) were added to Pt colloidal aqueous solution, and the slurry was then sonicated for 3 h at room temperature. The precipitates were separated by centrifugation, washed with water and ethanol, and dried in an oven at 100 °C in succession, and then were calcined at 300 °C for 2 h in air.

For the preparation of nanodevices, the CeO_2 NWs were dispersed on SiO_2/Si substrate which had Au contact pads (200 nm in thickness) predeposited by UV lithography and thermal evaporation. The patterns were made by using a focused ion beam (FIB) system with SEM capability. Pt contacts were directly written by FIB to bridge the CeO_2 NWs (or Pt NCs/CeO_2 NWs) to the Au pads. Finally, two Au pads were connected with a support chip by a Au wire binding technique. In order to obtain the information from the same CeO_2 NW before and after supporting Pt NCs, the CeO_2 NW nanodevice was dipped into the Pt colloidal aqueous solution and sonicated for 3 h. And then, the nanodevice was washed with water and ethanol, and then was calcined at 300 °C for 2 h in air.

The microstructures and morphology of CeO_2 NWs were characterized by X-ray diffraction (XRD, D8 Advanced) and scanning electron microscopy (SEM, Sirion FEG). Transmission electron microscopy (TEM) and EELS measurements were performed at a 200 kV JEOL 20l0F field emission TEM equipped with a Gatan electron energy loss spectrometer. The XPS measurements were carried out on a VG ESCA-LAB210 instrument using Al Kα irradiation. The ABM/350/6 UV lithography system and FEI Strata DB235 FIB system have been used to fabricate the Pt electrodes.

Gas-sensing properties of the samples were examined at room temperature. The testing gases employed in this work were pure air and 50−200 ppm CO in air. The gas-sensing response of the nanodevice was defined as the ratio of the electrical resistance in air (R_a) to that in testing gas (R_g). The sample resistance as a function of time was measured by using a Keithley 4200 SCS semiconductor characterization system.

Results and Discussion

A low-magnification SEM image (Figure 1a) shows that the CeO_2 NWs are several micrometers in length and about 50 nm in diameter. Figure 1b displays the XRD pattern of the sample. As can be seen from this figure, all diffraction peaks conform to a pure CeO_2 phase (fluorite structure, JCPDS 34-0394, space group $Fm\bar{3}m$).

Figure 2a exhibits a TEM image of a bundle of pure CeO_2 NWs, with clear surface and uniform length and diameter. Figure 2b shows a high-resolution TEM (HRTEM) image of one CeO_2 NW together with a fast Fourier transform (FFT) analysis (inset). According to the FFT analysis, three kinds of lattice fringe directions attributed to [111], [002], and [220] are obtained. The corresponding planes have interplanar spacings of 0.32, 0.28, and 0.19 nm, respectively, as measured from the HRTEM image. The NWs show a 1D growth along [110].[17] Figure 2c shows the TEM analysis of the as-prepared Pt NCs/CeO_2 NWs. It is clear that Pt NCs (dark dots in the Figure 2c) were highly dispersed on the CeO_2 NW with the mean diameter 3.5 ± 1.5 nm (Figure 2d). Moreover, the appearance of few Pt NCs on the carbon film of the TEM grid (Figure 2c) indicates a strong cohesion between Pt NCs and CeO_2 NWs. This implies that some interaction may happen between Pt NCs and CeO_2 NWs.

To understand the reactions and chemical information on the interface between Pt NCs and CeO_2 NWs, EELS analysis was

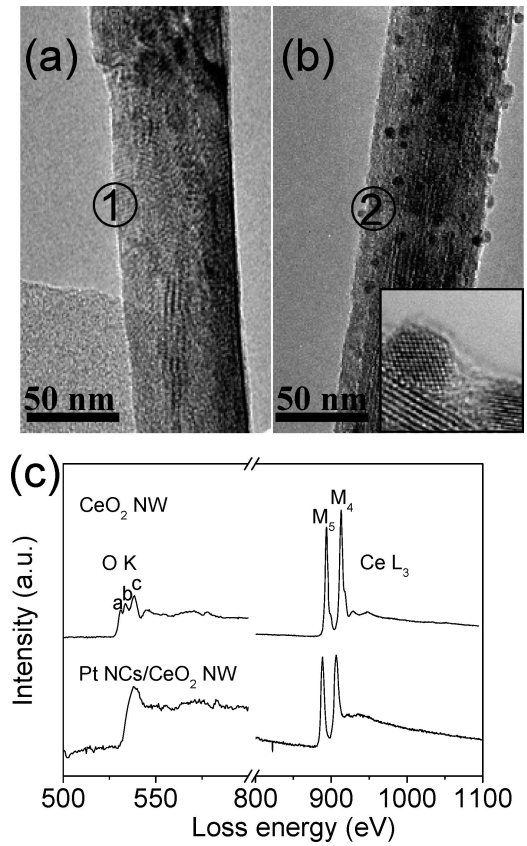

Figure 3. (a) TEM image of a single CeO_2 NW, (b) TEM image of a single Pt NC/CeO_2 NW, and (c) EELS spectra taken from sections 1 and 2, respectively.

performed. The EELS data were routinely obtained from the edge of an individual NW using the typical electron probe of a diameter of ~2 nm (full width at half-maximum) and a ca. 2 nA probe current. Parts a and b of Figure 3 exhibit the morphology comparison between a CeO_2 NW and a Pt NCs/CeO_2 NW. The HRTEM image of Pt NCs is shown in the bottom inset of Figure 3b. Figure 3c shows the EELS data taken from two regions: the clean edge of CeO_2 NWs (region 1) and the edge of CeO_2 NWs with Pt NCs (region 2), shown in Figure 3 parts a and b, respectively. The EELS Ce L_3 edge spectrum of region 1 is close to that of Ce^{4+}, whereas the spectrum of region 2 is close to that of Ce^{3+} based on the intensity ratios of M_5/M_4 (0.93 for region 1 and 1.10 for region 2). From these two ratios, the fractions of Ce^{3+} in the two regions were estimated to be 5% and 42%, respectively.[20,21] The O K edge spectra of CeO_2 NW and Pt NCs/CeO_2 NW also show different shapes. For pure CeO_2 NW, the edge has sharp peaks a, b, and c at 529.3, 532.0, and 536.2 eV, respectively. However, the relative intensities of the peaks a and b decrease as shown in the spectrum of the Pt NCs/CeO_2 NW O K edge. The Ce L_3 edge and O K edge peaks in the Pt NCs/CeO_2 NWs indicate that a certain amount of Ce^{4+} turns into Ce^{3+} and some oxygen vacancies might be produced because of the interaction of Pt NCs on CeO_2 NWs.[22,23]

Figure 4a depicts typical XPS spectra of the as-synthesized CeO_2 NWs and Pt NCs/CeO_2 NWs. The peak at 284.6 eV was attributed to ethanol and/or CO adsorbed on the surface of the CeO_2 NWs. In Figure 4b, we can find six Ce(3d) binding energy peaks of CeO_2 NWs which is consistent with the previous report of Ce^{4+},[4] indicating that the main valence of cerium in these samples was +4. Strikingly, the spectrum of Pt NCs/CeO_2 NWs exhibits more intense peaks at 885.3 and 903.4 eV (characteristic peaks of Ce_2O_3), compared to CeO_2 NWs, revealing that Pt NCs/

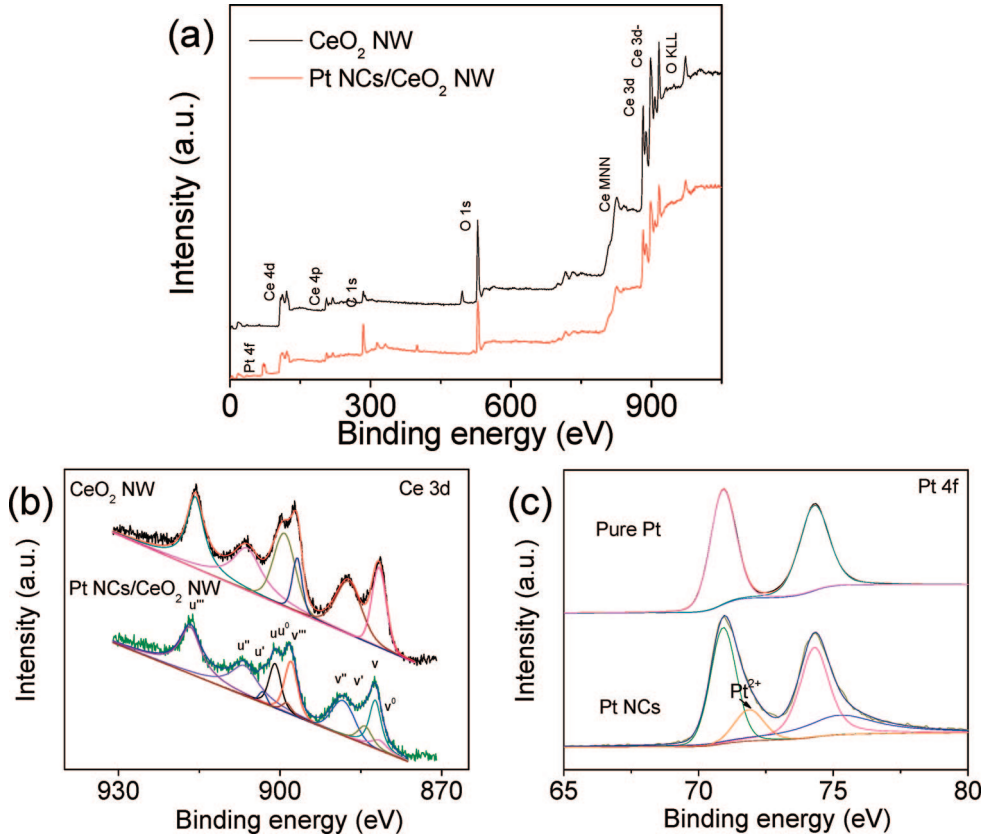

Figure 4. (a) Broad XPS spectra of CeO_2 NW before and after Pt was supported on; (b) XPS spectra of Ce 3d; (c) XPS spectra of Pt 4f.

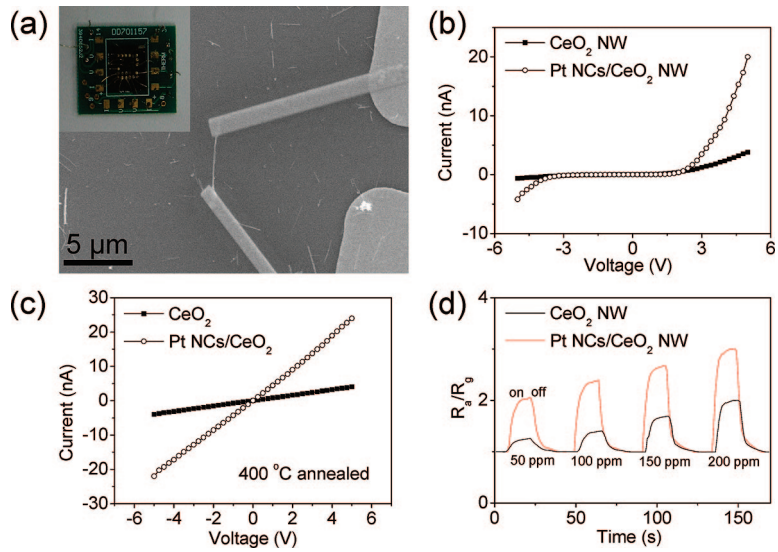

Figure 5. (a) SEM image of a single CeO_2 NW gas sensor, inset showing an optical image of the NW sensor chip; $I-V$ curves of a single CeO_2 NW and a single Pt NC/CeO_2 NW before (b) and after annealing at 400 °C for 1 h (c). (d) The gas sensibility response curves of a single CeO_2 NW and a single Pt NCs/CeO_2 NW, after being annealed, for different CO concentrations.

CeO_2 NWs contained more Ce^{3+}. This further convinces our statement based on the EELS investigation.

XPS data of the Pt(4f) core level region in pure Pt metal and Pt/CeO_2 NWs are given in Figure 4c. The spectrum for the pure Pt surface demonstrates no more than the metallic Pt(4f) doublet peaks, whereas in the Pt NCs/CeO_2 samples, the Pt(4f) region shows some additional peaks caused by multiple states. In this work, the Pt($4f_{7/2,5/2}$) peaks for the Pt NCs/CeO_2 NWs were deconvoluted into two sets of spin−orbit doublets. Accordingly, the Pt($4f_{7/2,5/2}$) peaks at 71.0 and 74.2 eV can be assigned to Pt metal and the peaks at 71.9 and 75.1 eV, respectively, are well-matched with Pt^{2+}.[24] A number of studies (mainly about catalysis works using high-area support materials) have reported that slightly oxidized noble metal is important to achieve high activity of dispersed Pt catalysts.[25–28]

An optical image of the NW sensor chip and an SEM image of a single CeO_2 NW gas sensor are shown in Figure 5a. Before the gas-sensing test, the electrical transport properties of the same CeO_2 NW before and after supporting Pt were investigated. Figure 5b displays the current−voltage ($I-V$) curves of the as-fabricated nanodevices (CeO_2 NW and Pt NCs/CeO_2 NW). Nonlinear behaviors were observed from the same CeO_2 NW before and after Pt NCs were supported. This could be due to some FIB-induced disorder produced underneath the Pt contacts during the contact fabrication process, which consequently introduces a multiphonon-assisted tunnel effect.[29,30] However, after annealing at 400 °C for 1 h in Ar gas for another nanodevice, which also has nonlinear electrical transport behavior before annealing, the $I-V$ curve shows clearly linear characteristics (Figure 5c), exhibiting good ohmic contacts between CeO_2 NW and Pt electrodes.[29,30] It is worth noting that the resistance of the Pt NCs/CeO_2 NWs (the Pt NCs were prepared on the CeO_2 NW nanodevice which had undergone annealing at 400 °C) is much lower than that of the pure CeO_2 NWs. Clearly, the incorporation of the Pt NCs can greatly improve the conductance of the NWs. Figure 5d shows the typical response curves of the CeO_2 NW sensor to CO gas after annealing at 400 °C. It can be seen that the single Pt NCs/CeO_2 NW sensor has a higher sensitivity to CO than that of the as-grown CeO_2 NW. The results indicate that introduction of Pt NCs on the surface of CeO_2 NW can significantly improve the gas sensitivity of the nanodevice. This enhancement of sensitivity has been further confirmed by comparing the gas sensitivities of an additional 15 pairs of CeO_2 NWs and Pt NCs/CeO_2 NWs.

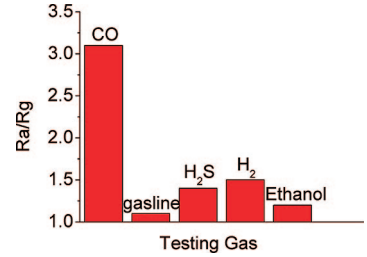

Figure 6. Sensitivity of Pt NCs/CeO_2 NW sensor to 200 ppm of different gases.

We also examined the response of the Pt NCs/CeO_2 NW sensor to different gases (at 200 ppm), such as CO, H_2, ethanol, gasoline, and H_2S under a heating voltage of 2 V. As shown in Figure 6, the sensitivities of Pt NCs/CeO_2 NW sensor to H_2, ethanol, gasoline, and H_2S are all much lower than that to CO. Conventional metal oxide sensors, mostly based on SnO_2, ZnO, etc., usually suffer from cross-sensitivity to other reducing gases though they have rather high sensitivity to CO.[14,15] In comparison with these sensors, the one based on Pt NCs/CeO_2 NW shows an obvious advantage in selective detection of CO gas.

For gas sensing, oxygen adsorption plays an important role in electrical transport properties of CeO_2 NWs. The adsorbed oxygen obtains conduction electrons from the CeO_2 NWs[15,31] and, therefore, lowers the conductance of CeO_2 NWs. When the sensors are exposed to reducing gases, for instance, CO or H_2S, the gases react with the adsorbed O^- and release the trapped electrons back to the conduction band, resulting in an increase of the conductance of CeO_2 NWs. Two possible mechanisms can be responsible for the enhanced sensitivity of the CeO_2 NWs after incorporation of Pt NCs according to the results. First, a local depletion area around Pt NCs may be formed on the surface of the NW due to charge transfer between Pt NCs and CeO_2 NWs.[14] Atomic oxygen species dissociating from Pt NCs possessing strong catalytic abilities can migrate onto the surface of the NW and hence increase the concentration of oxygen species per unit surface area in the air. Therefore, metal oxides supporting Pt NCs are active for the oxidation of

CO. CO can be adsorbed around the edges, corners, and steps of Pt particles particularly when the size of the Pt particles is below 10 nm.[26,32–34] In this study, the sizes of most Pt NCs are around 3.5 nm according to TEM observations. When the CO gas was introduced into the chamber, the enhanced reactions could reduce the concentration of preadsorbed O^- per unit surface area so that many more surface electrons were released into the NWs. This should be the most important contribution to the high sensitivity. Because the chemical activity of CeO_2 NWs was enhanced after supporting Pt NCs, the reaction between CO and O^- could therefore take place instantly and the efficiency of the reaction could be increased. The other mechanism could be that there are many oxygen vacancies on the surface of CeO_2 NW after Pt NCs are supported according to the XPS and EELS results. The oxygen vacancies act as donors in CeO_2 providing electrons to the conduction band of CeO_2. The existence of a large amount of vacancies in CeO_2 NWs induces stronger adsorptions of oxygen, leading to an increase of the conductance.

Conclusion

In conclusion, a new nanodevice using a single CeO_2 NW as the sensing unit was successfully fabricated. The gas sensitivity can be significantly increased by incorporation of Pt NCs on a CeO_2 NW. The studies on the microstructure and surface bonding states for both kinds of samples reveal that the strong adsorption (to CO) of the very fine Pt NCs on CeO_2 NW and the charge transfer between the Pt NCs and CeO_2 NW are the most important contributions to the high gas sensitivity of the Pt NCs/CeO_2 NW sensor. On the basis of the excellent chemical stability of CeO_2 and its high gas-sensing behaviors, the Pt NCs/CeO_2 NW sensor is expected to have promising applications in various complicated environments for fast detection of poisonous gases.

Acknowledgment. This work was supported by the NSFC (Grants 10575078, 10775110, and 20221101) and the MOE of China (Grant NCET-04-0671).

References and Notes

(1) *Catalysis by Ceria and Related Materials*; Trovarelli, A., Ed.; Dunod: London, 2002.
(2) Powell, B. R.; Bloink, R. L.; Eickel, C. C. *J. Am. Ceram. Soc.* **1988**, *71*, 104.
(3) Kaspar, J.; Fornasiero, P.; Graziani, M. *Catal. Today* **1999**, *50*, 285.
(4) Si, R.; Zhang, Y. W.; Li, S. J.; Lin, B. X.; Yan, C. H. *J. Phys. Chem. B* **2004**, *108*, 12481.
(5) Steele, B. C. H. *Nature* **1999**, *400*, 619.
(6) Atkinson, A.; Barnett, S.; Gorte, R. J.; Irvine, J. T. S.; Mcevoy, A. J.; Mogensen, M.; Singhal, S. C.; Vohs, J. *Nat. Mater.* **2004**, *3*, 17.
(7) Masui, T.; Fujiwara, K.; Machida, K. I.; Adachi, G. Y. *Chem. Mater.* **1997**, *9*, 2197.
(8) Zhang, Y. W.; Si, R.; Liao, C. S.; Yan, C. H.; Xiao, C. X.; Kou, Y. *J. Phys. Chem. B* **2003**, *107*, 10159.
(9) Si, R.; Zhang, Y. W.; You, L. P.; Yan, C. H. *Angew. Chem., Int. Ed.* **2005**, *44*, 3256.
(10) Yuan, Q.; Liu, Q.; Song, W. G.; Feng, W.; Pan, W. L.; Sun, L. D.; Zhang, Y. W.; Yan, C. H. *J. Am. Chem. Soc.* **2007**, *129*, 6698.
(11) Fu, X. Q.; Wang, C.; Yu, H. C.; Wang, Y. G.; Wang, T. H. *Nanotechnology* **2007**, *18*, 145503.
(12) Kong, J.; Chapline, M.; Dai, H. *Adv. Mater.* **2001**, *13*, 1384.
(13) Choi, H. C.; Shim, M.; Bangsaruntip, S.; Dai, H. J. *J. Am. Chem. Soc.* **2002**, *124*, 9058.
(14) Kolmakov, A.; Klenov, D. O.; Lilach, Y.; Stemmer, S.; Moskovits, M. *Nano Lett.* **2005**, *5*, 667.
(15) Liao, L.; Lu, H. B.; Li, J. C.; He, H.; Wang, D. F.; Fu, D. J.; Liu, C.; Zhang, W. F. *J. Phys. Chem. C* **2007**, *111*, 1900.
(16) Liao, L.; Lu, H. B.; Li, J. C.; Liu, C.; Fu, D. J.; Liu, Y. L. *Appl. Phys. Lett.* **2007**, *91*, 173110.
(17) Mai, H. X.; Sun, L. D.; Zhang, Y. W.; Si, R.; Feng, W.; Zhang, H. P.; Liu, H. C.; Yan, C. H. *J. Phys. Chem. B* **2005**, *109*, 24380.
(18) Teranishi, T.; Hosoe, M.; Tanaka, T.; Miyake, M. *J. Phys. Chem. B* **1999**, *103*, 3818.
(19) Rioux, R. M.; Song, H.; Hoefelmeyer, J. D.; Yang, P.; Somorjai, G. A. *J. Phys. Chem. B* **2005**, *109*, 2192.
(20) Wu, L. J.; Wiesmann, H. J.; Moodenbaugh, A. R.; Klie, R. F.; Zhu, Y. M.; Welch, D. O.; Suenaga, M. *Phys. Rev. B* **2004**, *69*, 125415.
(21) Gilliss, S. R.; Bentley, J.; Carter, C. B. *Appl. Surf. Sci.* **2005**, *241*, 61.
(22) Garvie, L. A. J.; Buseck, P. R. *J. Phys. Chem. Solids* **1999**, *60*, 1943.
(23) Akita, T.; Okumura, M.; Tanaka, K.; Kohyama, M.; Haruta, M. *Catal. Today* **2006**, *117*, 62.
(24) Bera, P.; Priolkar, K. R.; Gayan, A.; Sarode, P. R.; Hegde, M. S.; Emura, S.; Kumashiro, R.; Jayaram, V.; Subbana, G. N. *Chem. Mater.* **2003**, *15*, 2049.
(25) Guzman, J.; Gates, B. C. *J. Am. Chem. Soc.* **2004**, *126*, 2672.
(26) Fu, Q.; Saltsburg, H.; Flytzani-Stephanopoulos, M. *Science* **2003**, *301*, 935.
(27) Fu, L.; Wu, N. Q.; Yang, J. H.; Qu, F.; Johnson, D. L.; Kung, M. C.; Kung, H. H.; Dravid, V. P. *J. Phys. Chem. B* **2005**, *109*, 3704.
(28) Zarraga-Colina, J.; Nix, R. M. *Surf. Sci.* **2006**, *600*, 3058.
(29) Mathur, S.; Barth, S.; Shen, H.; Pyun, J. C.; Werner, U. *Small* **2005**, *1*, 713.
(30) Nam, C. Y.; Tham, D.; Fischer, J. E. *Nano Lett.* **2005**, *5*, 2029.
(31) Wan, Q.; Li, Q. H.; Chen, Y. J.; Wang, T. H.; He, X. L.; Li, J. P.; Lin, C. L. *Appl. Phys. Lett.* **2004**, *8*, 3654.
(32) Rolison, D. R.; Hagans, P. L.; Swider, K. E.; Long, J. W. *Langmuir* **1999**, *15*, 774.
(33) Boccuzzi, F.; Chiorino, A.; Manzoli, M.; Lu, P.; Akita, T.; Ichiawa, S.; Haruta, M. *J. Catal.* **2001**, *202*, 256.
(34) Mori, K.; Hara, T.; Mizugaki, T.; Ebitani, K.; Kaneda, K. *J. Am. Chem. Soc.* **2004**, *126*, 10657.

JP7117778